EIC Detector R&D Progress Report

Project ID: eRD14

Project Name: PID Consortium for an integrated program for Particle Identification (PID) at a future Electron-Ion Collider

Period Reported: from 7/1/2017 to 12/31/2017

Contact Persons: Pawel Nadel-Turonski and Yordanka Ilieva

Project Members:

M. Alfred[10], L. Allison[18], M. Awadi[10], B. Azmoun[3], F. Barbosa[13], M. Boer[16], W. Brooks[20], T. Cao[24], M. Chiu[3], E. Cisbani[13,14], M. Contalbrigo[12], S. Danagoulian[17], A. Datta[23], A. Del Dotto[13,24], M. Demarteau[2], A. Denisov[11], J.M. Durham[16], A. Durum[11], R. Dzhygadlo[9], D. Fields[23], Y. Furletova[15], C. Gleason[24], M. Grosse-Perdekamp[22], J. Harris[25], X. He[8], H. van Hecke[16], T. Horn[4], J. Huang[3], C. Hyde[18], Y. Ilieva[24], G. Kalicy[4], A. Kebede[17], B. Kim[5], E. Kistenev[3], Y. Kulinich[22], M. Liu[16], R. Majka[30], J. McKisson[15], R. Mendez[20], I. Mostafanezhad[21], P. Nadel-Turonski[19], K. Park[15], K. Peters[9], T. Rao[3], R. Pisani[3], W. Roh[8], P. Rossi[15], M. Sarsour[8], C. Schwarz[9], J. Schwiening[9], C.L. da Silva[16], N. Smirnov[25], J. Stevens[6], A. Sukhanov[3], X. Sun[8], S. Syed[8], J. Toh[22], R. Towell[1], T. Tsang[3], G. Varner[21], R. Wagner[2], C. Woody[3], C.-P. Wong[8], W. Xi[15], J. Xie[2], Z.W. Zhao[7], B. Zihlmann[15], C. Zorn[15].

[1] Abilene Christian University, Abilene, TX 79601
[2] Argonne National Lab, Argonne, IL 60439
[3] Brookhaven National Lab, Upton, NY 11973
[4] Catholic University of America, Washington, DC 20064
[5] City College of New York, New York, NY 10031
[6] College of William & Mary, Williamsburg, VA 2318
[7] Duke University, Durham, NC 27708
[8] Georgia State University, Atlanta, GA 30303
[9] GSI Helmholtzzentrum für Schwerionenforschung GmbH, 64291 Darmstadt, Germany
[10] Howard University, Washington, DC 20059
[11] Institute for High Energy Physics, Protvino, Russia
[12] INFN, Sezione di Ferrara, 44100 Ferrara, Italy
[13] INFN, Sezione di Roma, 00185 Rome, Italy
[14] Istituto Superiore di Sanità, 00161 Rome, Italy
[15] Jefferson Lab, Newport News, VA 23606
[16] Los Alamos National Lab, Los Alamos, NM 87545
[17] North Carolina A&T State University, Greensboro, NC 27411
[18] Old Dominion University, Norfolk, VA 23529
[19] Stony Brook University, Stony Brook, NY 11794
[20] Universidad Técnica Federico Santa María, Valparaíso, Chile
[21] University of Hawaii, Honolulu, HI 96822
[22] University of Illinois, Urbana-Champaign, IL 61801
[23] University of New Mexico, Albuquerque, NM 87131
[24] University of South Carolina, Columbia, SC 29208
[25] Yale University, New Haven, CT 06520

Abstract

Excellent particle identification (PID) is an essential requirement for a future Electron-Ion Collider (EIC) detector. Identification of the hadrons in the final state is critical to study how different quark flavors contribute to nucleon properties. Reliable identification of the scattered electron is important for covering kinematics where pion backgrounds are large. The EIC PID consortium (eRD14) was formed to develop an integrated PID program using a suite of complementary technologies covering different ranges in rapidity and momentum, as required by the asymmetric nature of the collisions at the EIC. The PID consortium has also worked closely with BNL and JLab to ensure that the specific R&D projects are compatible with the detector concepts that are being pursued there.

Table of Contents

1. Introduction

Identification of hadrons in the final state is essential for key EIC measurements formulated in the EIC White Paper and referenced in the NSAC Long Range Plan. These include 3D imaging of the nucleon in momentum space through semi-inclusive DIS (where flavor tagging can tell us about the transverse momentum distributions and, potentially, the orbital angular momentum of the strange sea), and open charm (with decays of D-mesons into kaons), which is important for probing the distribution of gluons in protons and nuclei.

Satisfying the PID requirements within the very asymmetric kinematics of the EIC (discussed in detail in the eRD14 proposal for FY17) requires a suite of detector technologies that can address the specific challenges (in terms of momentum coverage, available space, *etc.*) encountered in various ranges of rapidity. Thus, the integrated PID program pursued by the eRD14 Consortium includes different detector systems for each endcap and the central barrel, as well as corresponding sensor and readout solutions. While we ensure compatibility with the detector concepts developed at BNL and JLab, all funded R&D being pursued by the consortium is conceptually novel. The dual-radiator RICH (dRICH) for the hadron endcap is the first such design for a solenoid-based collider detector. The modular aerogel RICH (mRICH), primarily intended for the electron endcap, introduces lens-based focusing, which improves momentum coverage and reduces the required sensor area. The compact, high-performance DIRC for the barrel combines new optics for spatial imaging with good timing (<100 ps) to allow a significant improvement in momentum coverage compared with the state-of-the-art. There is also an effort to develop high-resolution (10 − 20 ps) time-of-flight detectors. The funded work on photosensors in high magnetic fields and on adaptation of LAPPDs to EIC requirements is also aimed at developing a new generation of devices. Starting in FY18, the sensor effort has been extended to include corresponding readout electronics.

In order to be able to coherently evolve one integrated concept, the key consortium goals for FY18 were to develop a baseline design for the dRICH satisfying the constraints of the proposed EIC detector(s); to build a second mRICH prototype with small pixels and larger focal length and test it in-beam, as well as implement the mRICH in JLab and BNL simulation frameworks; to perform an in-beam test and evaluate the performance of the new, advanced cylindrical lens for the DIRC and to further refine the algorithms for time-based reconstruction. The high-B photosensor and LAPPD efforts have continued, and the new readout-electronics activities by the Hawaii group and INFN are on track to deliver a first set of devices for the mRICH test beam at Fermilab in the early summer of 2018. There has also been a targeted effort on electronics development for the high-resolution TOF.

2. Hadron Identification

2.1 Summary

The funded R&D on the three Cherenkov systems has been proceeding very well, and they all promise significant advances over the fallback options (single-radiator gas RICH for the dRICH, proximity-focusing aerogel RICH for the mRICH, or a DIRC geared only towards spatial imaging or timing). The mRPC-based high-resolution TOF received only limited funding in FY18, which was used for electronics developments by a new institution joining the consortium.

2.2 Dual-Radiator RICH (dRICH)

The goal of the dRICH detector is to provide good hadron separation (π/K/p) over a momentum range between 3 and 50 GeV/*c* (for π/K), in the forward, ion-side region of the EIC detector.

2.2.1 Past

2.2.1.1 What was planned for this period?

The overall goal for FY18 was to establish a baseline design for the dRICH, a dual-radiator (aerogel and gas) RICH with outward reflecting mirrors, in configurations adapted to match the space available in both the JLab and BNL detector concepts. This included an adaptation of the dRICH design to the latter geometry, and a characterization of its performance. In addition, work was carried out on the reconstruction software, and on the focal-plane design. The latter included tessellated photosensors to reduce the spherical aberration of the mirror, and further evaluation of possible photosensor options. All these activities will continue through May 2018.

The last of the planned activities, which will continue in early 2018, is to exploit synergies with the eRD6 effort on the gas RICH, for which the dRICH reconstruction package would be adapted. Furthermore, an evaluation of the performance of the gas RICH will be done using the same tools as used for the dRICH. This effort is carried out in collaboration with eRD6 members working on the EIC detector-concept based on sPHENIX.

2.2.1.2 What was achieved?

All the goals were achieved as planned and the work is on track. A baseline design for the dRICH detector has been implemented in GEMC, and the so called Inverse Ray Tracing (IRT) algorithm (see [1]) has been adopted to characterize the system and evaluate its performance (see FY18 eRD14 proposal, section 2.2, for details). The reconstruction software has been coded as a C++ class that can be easily used in different frameworks (*e.g.*, GEMC, fun4all, and eicROOT), providing a fast and effective way to characterize RICH systems and to provide performance estimates.

An important application of the reconstruction software is the above-mentioned synergy with the

eRD6 gas RICH, for which the IRT class was used (in combination with an implementation of the gas RICH in the ePHENIX simulation framework) for characterize and evaluate the performance of the gas RICH. The latter uses CF_4 gas and inward reflecting mirrors arranged in eight sectors. Each sector has a GEM-based photosensor plane, sensitive mainly in the UV. The main advantage of the GEMs is that regular photosensors would not be able to operate in the area of high radiation and high magnetic field near the beam on the outgoing hadron side. However, using such short wavelengths makes the RICH sensitive to chromatic effects in the gas. It also precludes the use of a dual-radiator configuration since aerogel is a strong scatterer in the UV – and with inward-reflecting mirrors it would have to be placed in front of the photosensors.

Figure 2.2.1 shows a simulated ePHENIX gas RICH (left) and the resolution of the system as a function of the particle momentum (right). The PID capability of the eRD6 gas RICH is shown in Fig. 2.2.2.

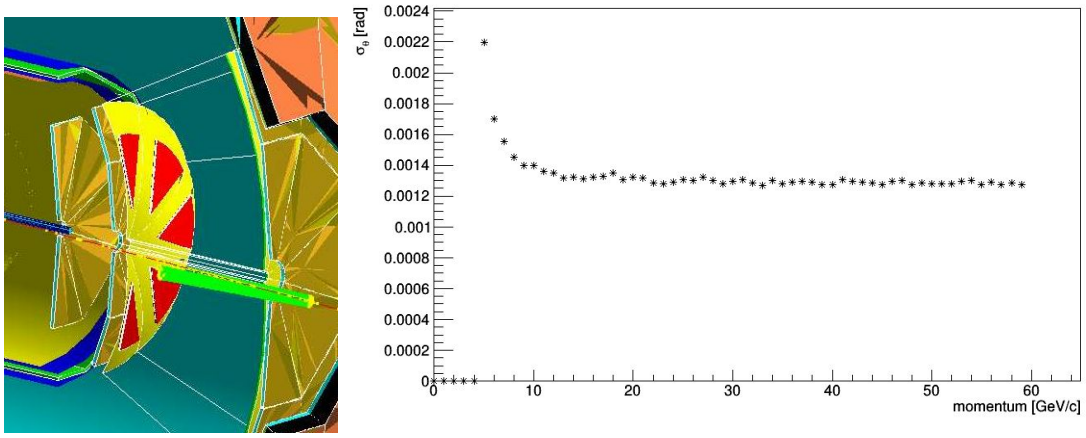

Figure 2.2.1: (Left panel) A section view of the ePHENIX gas RICH: the GEM-based detector planes are shown in red; (Right panel) the Cherenkov angular resolution of the system as a function of particle momentum (using pions). The sigma contains all the relevant error sources (chromatic dispersion, pixel size (3 mm) and track bending in the magnetic field). The dominant error for this inward-reflecting mirror configuration is the chromatic dispersion, which is of the order of 0.9 mrad. This result has been obtained applying the IRT algorithm to a sample of 10k pion tracks and adopting the quantum efficiency of a GEM-based photon detector [2].

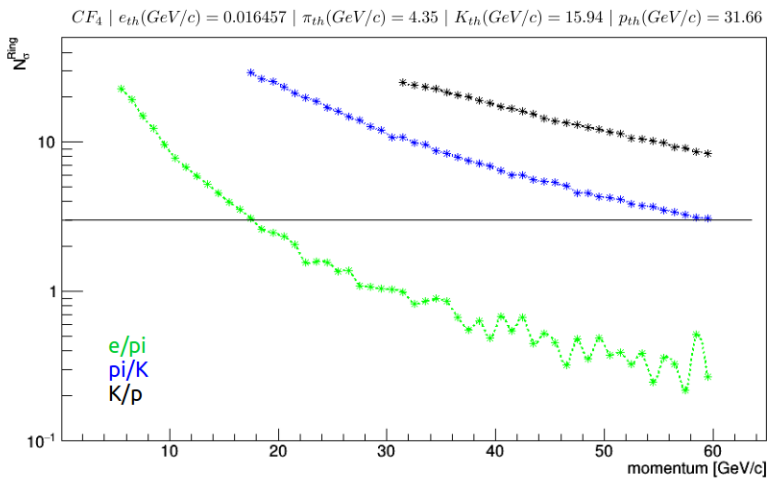

Figure 2.2.2: Particle separation power at 10° for the CF_4 gas RICH in terms of number of standard deviations, N_σ .

A preliminary study of a dRICH detector (aerogel and gas) adapted to fit the available space in ePHENIX (as well as the BeAST) is shown in Fig. 2.2.3. The simulation was made using GEMC, but an implementation in other frameworks is straightforward.

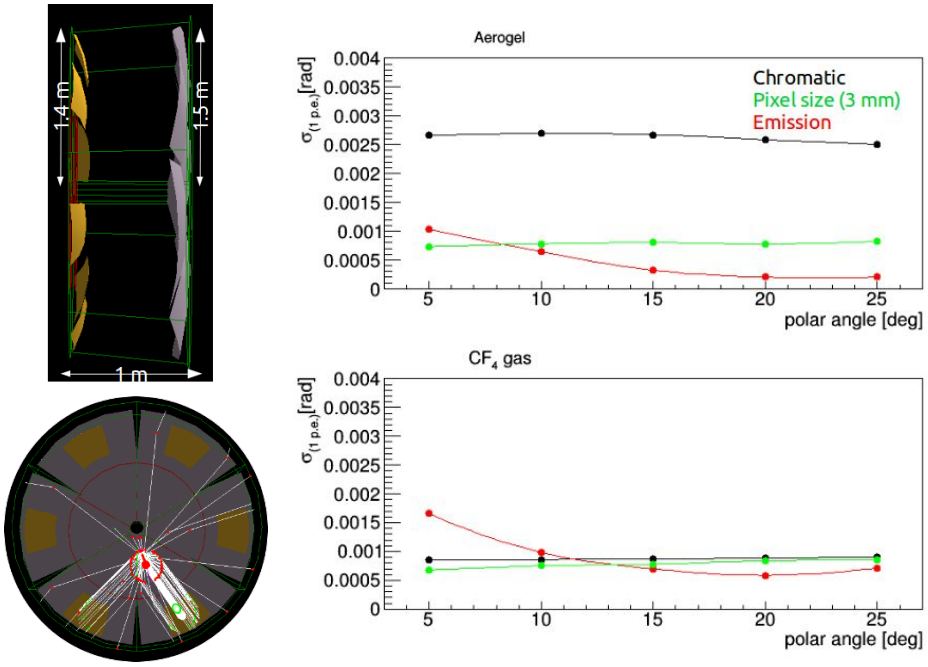

Figure 2.2.3: (Left side) Detector geometry in GEMC (Geant4); (Right side) Angular dispersion contributions as a function of the polar angle of the track; the outward-reflecting mirror configuration can cause an increase of the emission error (due to a mismatch between the focal plane of a spherical mirror and the sensors) - but this can be managed through careful design of the sensor plane. However, even the preliminary design shows that the emission error in the dRICH is only significant at small angles. CF_4 gas is shown here only for comparison with the gas RICH.

The PID capability of an ePHENIX/BeAST type dRICH with C_2F_6 gas is shown in Fig. 2.2.4.

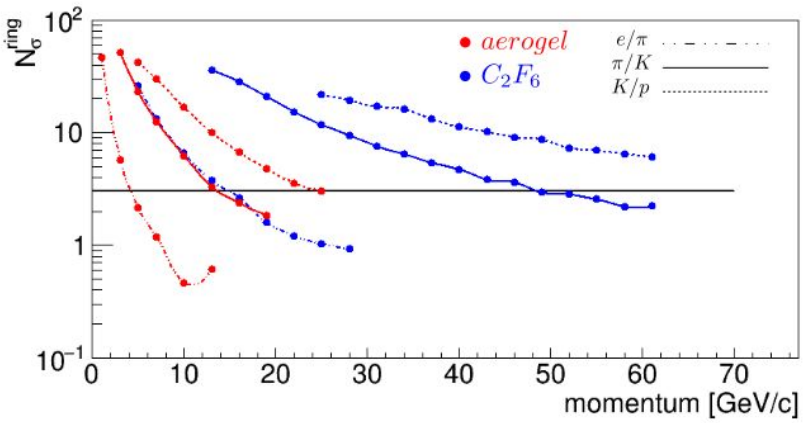

Figure 2.2.4: Separation power at 10° of a dRICH (C_2F_6 gas and aerogel with n = 1.02) with ePHENIX-like dimensions.

A direct comparison between the two systems is shown in Fig. 2.2.5. The gas RICH (left) can be combined with partial coverage provided at large angles by a ring of mRICH detectors providing partial coverage at large angles as well as TOF detectors.

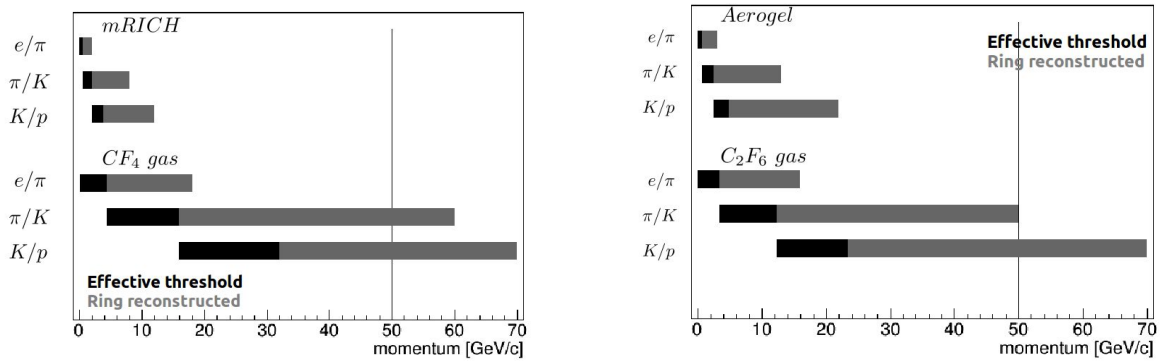

Figure 2.2.5: (Left panel) The momentum coverage of the gas RICH system is shown when assumed in combination with mRICH placed in the hadron endcap; "effective threshold" highlights the region in which particle species can be separated only by threshold, whereas the gray part of the bars stands for having a ring for each of the two particle species. (Right panel) Momentum coverage of an ePHENIX-like dRICH.

The dRICH is designed to provide continuous momentum coverage in RICH mode (*i.e.*, with the rings fully reconstructed). The C_2F_6 gas is chosen to match the refractive index of the aerogel (it also scintillates less than CF_4, but this is secondary). The use of a heavier gas is a trade-off between a few GeV/*c* at the top of the range and a better coverage in the overlap region. The design also tried to optimize the photosensor area, which is common to both the gas and aerogel radiators.

The CF_4 gas RICH, on the other hand, was designed to reach the maximum possible momentum, even though the need to use GEMs close to the beam means that despite using a gas with very low refractive index, the momentum reach is limited by chromatic effects (*i.e.*, changes in the refractive index of the gas at short wavelengths). The geometry of the mirrors allows for an outer ring of mRICH detectors, but the choice of CF_4 gas leaves a gap in the p/K identification, and an overlap in π/K coverage is only provided by using the gas RICH in threshold mode (*i.e.*, by only counting the total number of photons without any ring reconstruction – identifying particles below a certain threshold as kaons and ones above as pions). In the central region, where there is not enough space for an mRICH detector, high-resolution (10–20 ps) TOF could be used. Since the momentum reach of the TOF is somewhat smaller than for the mRICH, it poses similar challenges in terms of continuous coverage. If one were willing to sacrifice the highest end of the momentum reach, one could change CF_4 to a heavier gas, as was done for the dRICH, but one would need to ensure that the new gas satisfies the requirements of the GEMs (transparency in the UV, low chromatic effects, *etc.*). One could also consider filtering out some of the shortest wavelengths to reduce the chromatic effects, but at the expense of a reduced photon yield.

There has been a lot of progress on the dRICH (and the gas RICH) studies, but in order to find

the best solution for particle ID in the hadron endcap, which is perhaps the most important and challenging aspect of a future EIC detector, more R&D will be needed. It will address the questions mentioned above, as well as integration of the proper sensor solutions, both with the RICH itself and in the EIC detector. Preliminary studies of the neutron flux suggest that the backgrounds in the location of the dRICH photosensors will be relatively modest, making it possible to use SiPMs. The PID performance with radiation-damaged SiPMs would need to be tested in a prototype. At the same time, if a magnetic-field tolerant LAPPD with pixelated readout is developed, it would also provide an ideal solution for the dRICH. As a fallback, commercially available MCP-PMTs fulfil the requirements, but are currently more expensive. For the gas RICH, UV-sensitive GEMs are the only option (the initial eRD14 proposal included R&D on GEMs sensitive at lower wavelengths, but the R&D was not funded).

2.2.2 Future

2.2.2.1 What is planned for the next funding cycle and beyond? How, if at all, is this planning different from the original plan?

The plan for the next funding cycle (up to May 2018) has two components: 1) the study of the dRICH performance in presence of physics backgrounds; 2) the synergic activity between eRD14 and eRD6 on RICH development. The detailed plan was the following:

- Study a physics channel of interest to the EIC in the presence of physics backgrounds.
- Evaluate of the dual-radiator RICH performance in such an extended (physics) context.
- Adapt the dRICH for the geometry currently used in the BNL concept detectors (and their magnetic field maps) to allow a direct comparison with the eRD6 gas RICH.

Concerning the third point, the work has already started and we already provided a first comparison between the two options. We also plan to study the dRICH (JLab-dRICH) performance using physical events simulated with PYTHIA, and a likelihood formulation will be added to the IRT algorithm providing the performance of the system.

It would be also important to lay the foundation for a physical analysis of the performance in the BNL detector context, to the extent that the limited time will allow.

2.2.2.2 What are the critical issues?

The work is progressing very well, but the postdoc funding ends in May of 2018. Thus, it is also critical to document all progress so that no results are lost.

References:

[1] Akopov, Norair, et al., *The HERMES dual-radiator ring imaging Cherenkov detector*, NIMA 479.2

(2002): 511530.

[2] Azmoun, B. et al., *Collection of photoelectrons and operating parameters of CsI photocathode GEM detectors*, IEEE Transactions on Nuclear Science 56.3 (2009): 1544-1549.

2.3 Modular Aerogel RICH (mRICH)

This lens-based, compact, and modular Aerogel RICH detector provides hadron PID capability with momentum coverage from 3 to 10 GeV/*c* (for π/K). The details of this detector design can be found in the eRD14 FY18 proposal. In this report, we highlight the progress made on the mRICH project since July of 2017 and describe further activities planned for FY18.

2.3.1 Past

2.3.1.1 What was planned for this period?

The planned major activities for this period included (1) the construction of the second mRICH (without the readout electronics) prototype and the preparation for the second mRICH beam test at Fermilab; (2) the implementation of the mRICH detector in the Forward sPHENIX experiment and in the BeAST EIC detector design; (3) the study of the mRICH performance in the JLab EIC detector design using Pythia events.

2.3.1.2 What was achieved?

The achieved tasks for the mRICH project during this report period include: (1) the first mRICH paper based on the first mRICH beam test (Fermilab, 2016) has been published in NIMA [1]; (2) two mRICH prototypes (one with a Fresnel lens, f = 6", and the other with a spherical lens, f = 8") as well as the beam hodoscope with full coverage were constructed, as shown in Fig. 2.3.1; (3) the updated mRICH detector was implemented in the Forward sPHENIX experiment (see Fig. 2.3.2) using the Fun4All framework (one of the proposed software frameworks to be considered for the EIC experiments); (4) the Pythia event generator was setup for the mRICH performance study in JLEIC, as shown on Fig. 2.3.3; (5) the concerted plan for developing the mRICH readout for the second beam test was put in action.

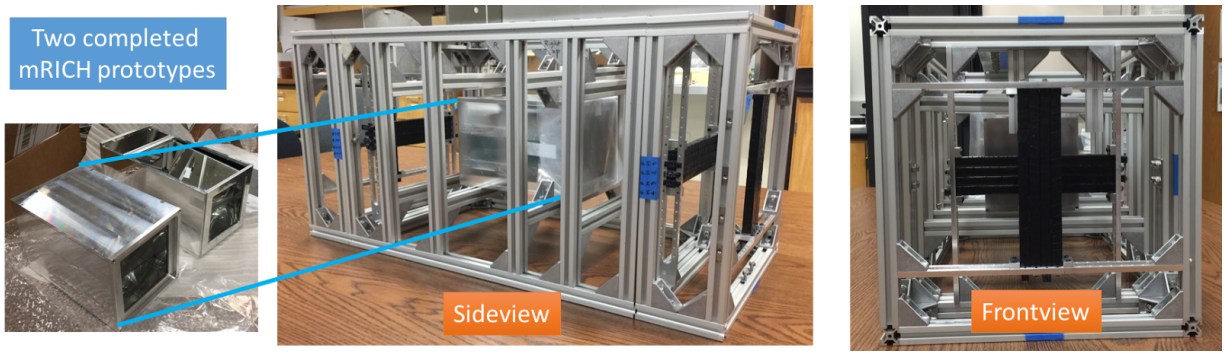

Figure 2.3.1: Completed mRICH teststand for a single-module test. Left picture shows the two mRICH prototypes (one with Fresnel lens, and the other with spherical lens); middle picture shows the side view of the teststand; and the right picture shows the front view with a partial installation of the finger hodoscope.

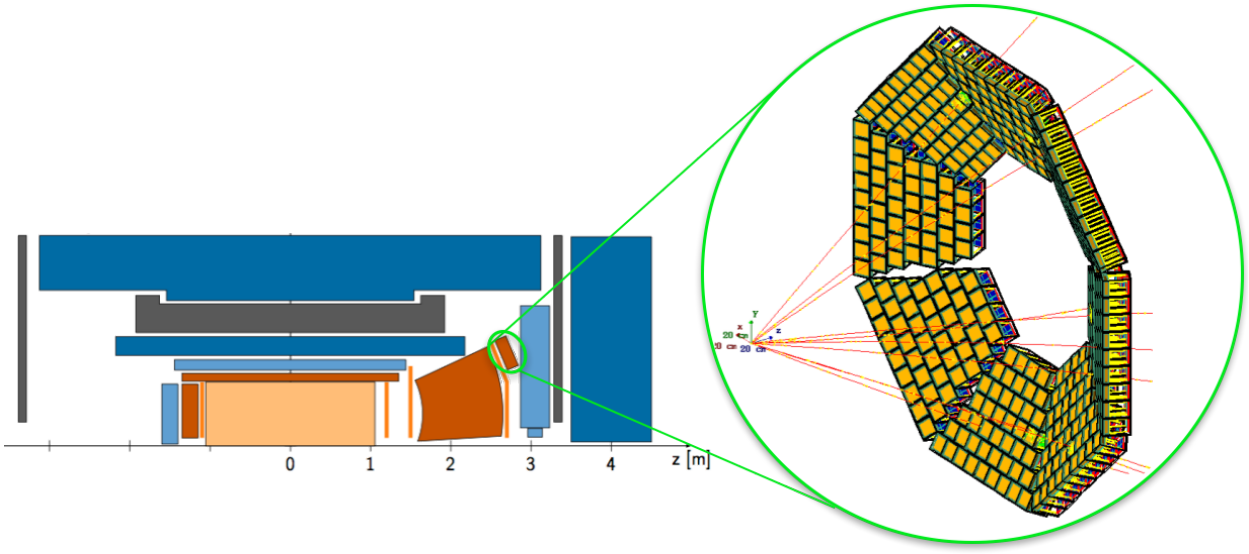

Figure 2.3.2: mRICH subsystem implemented (using Fun4all software) within the sPHENIX detector design (shown on the left). The individual mRICH modules can be mounted projectively toward the interaction point.

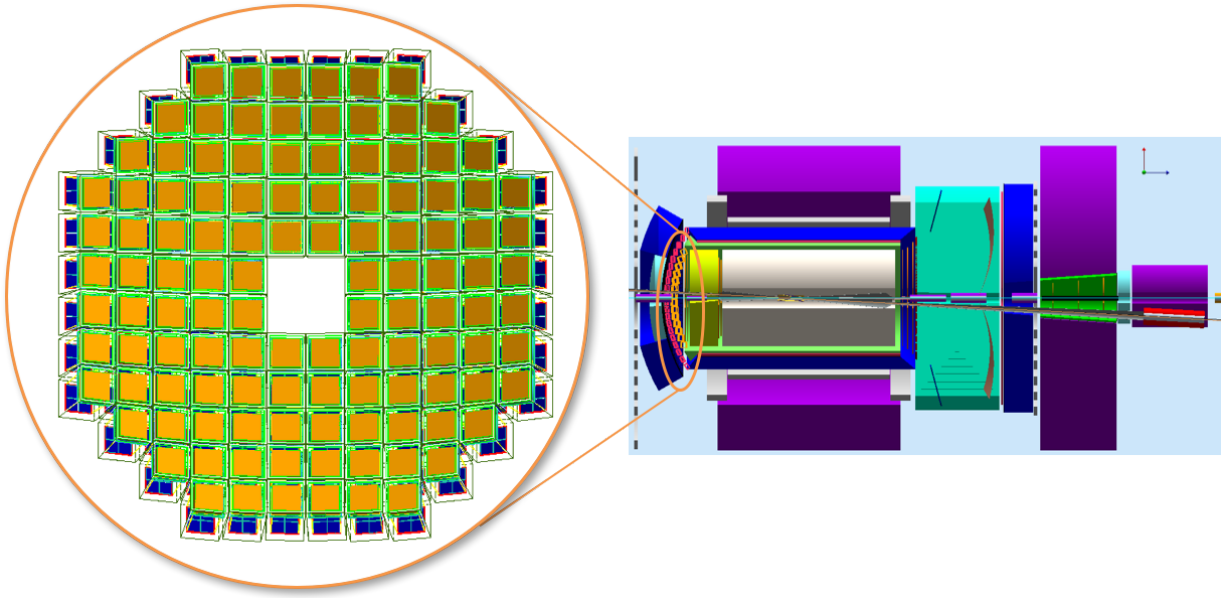

Figure 2.3.3: mRICH subsystem implemented in GEMC within the JLab detector design (shown on the right). The individual mRICH modules can be mounted projectively toward the interaction point.

2.3.1.3 What was not achieved, why not, and what will be done to correct?

We need to procure aerogel blocks for the second beam test. Lack of funding is the major issue.

2.3.2 Future

2.3.2.1 What is planned for the next funding cycle and beyond? How, if at all, is this planning different from the original plan?

The major activity in the next funding cycle is to successfully complete the second mRICH beam test in order to demonstrate the PID capability of π/K separation and to publish the results. A possible run configuration is to take data with the two mRICH modules installed in tandem, assuming we will have two independent readout systems ready for the test as shown in Fig. 2.3.4, with a common set of beam hodoscope.

In the coming budget period, the mRICH group plans to look into the options for a radiation-hard Fresnel lens.

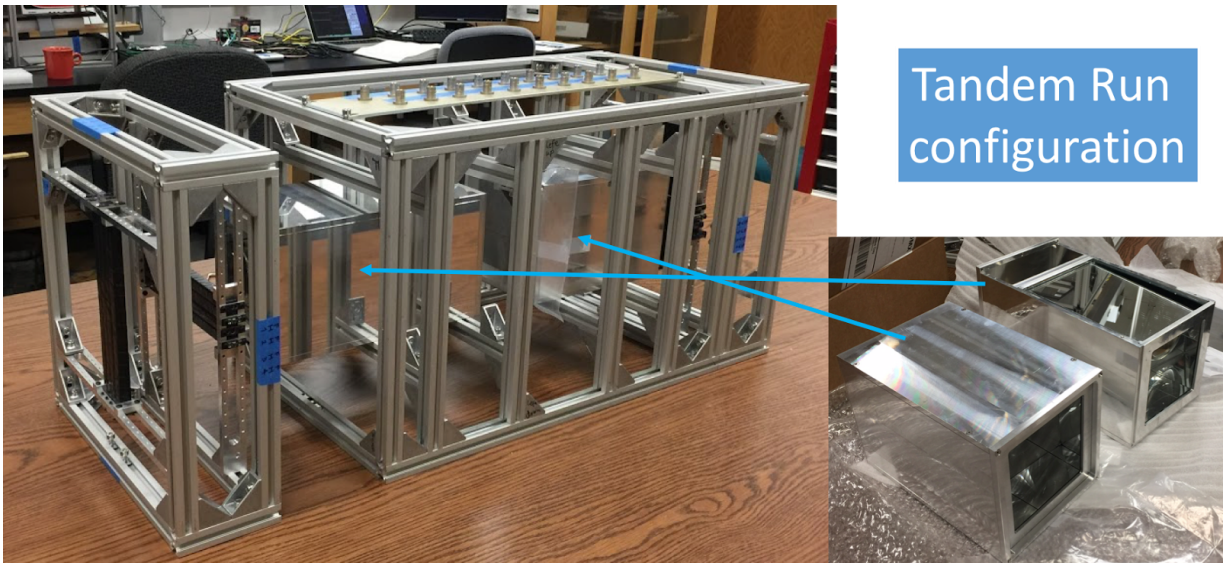

Figure 2.3.4 A possible mRICH run configuration (no readout electronics included yet) for testing the two mRICH prototypes in parallel.

2.3.2.2 What are the critical issues?

The success of the second mRICH beam test in FY18 is critically contingent upon the readiness of the readout systems, which are currently under the development in parallel by two groups within the eRD14 Consortium. The plan is that we will be able to readout the mRICH both with Hamamatsu H13700 multi-anode PMT's and with MPPC arrays. Exploring the single-photon measurement capability using MPPC arrays is important for the PID group to identify the photosensor technology to be operated in a strong magnetic field environment. See section 3.4 on the readout electronics development for details.

References

[1] C.P. Wong, et. al., *Modular focusing ring imaging Cherenkov detector for electron-ion collider experiment,* NIM A 871, 13 (2017).

2.4 High Performance DIRC

A radially-compact detector based on the DIRC (Detection of Internally Reflected Cherenkov light) principle is a very attractive solution for the EIC, providing particle identification (e/π, π/K, K/p) over a wide momentum range. The DIRC is a type of RICH detector using rectangular-shaped radiators made of synthetic fused silica that also function as light guides transporting the Cherenkov photons to an expansion volume, where they are recorded by an array of photon sensors. During the photon transport the emission angle of Cherenkov photons with respect to the particle track is maintained and can be reconstructed from measured parameters. DIRC detectors are inherently 3D devices, measuring the image location on the detector surface (*x, y*) and the time of arrival of each photon (*t*).

The High Performance DIRC design developed for the EIC detector is inspired by the original DIRC detector used by BaBar, and the PANDA Barrel DIRC detector currently in development. The baseline design, implemented in a Geant4 simulation, is shown in Fig. 2.4.1a. The radiators are 4.2-m long each, with a cross-section of 17 mm x 32 mm. Eleven such bars are placed side-by-side, separated by a small air gap, into a bar box. The 16 bar boxes are arranged in a barrel with a radius of 1 m around the beam line. Mirrors are attached to one end of each bar. On the opposite end, where photons exit the bar, a special 3-layer spherical lens is attached to each bar. The other side of the 3-layer lens is coupled to a large prism-shaped expansion volume, made of synthetic fused silica. A closeup view of this region is shown in Fig. 2.4.1b. The prism has a 38° opening angle, and dimensions 285 mm x 390 mm x 300 mm. The detector plane of each prism is covered by 2 mm x 2 mm pixels for a total of about 450k channels to record the location and arrival time of the Cherenkov photons.

A key component to reach the required performance is a special 3-layer spherical compound lens. A schematic and photos of a prototype lens, procured in 2015, are shown in Fig. 2.4.1c. This lens contains a layer of the high-refractive index material Lanthanum crown glass (NLaK33), sandwiched between two layers of synthetic fused silica. The two radii of the 3-layer lens were optimized to remove aberrations present in standard lenses by first defocusing and then focusing the photons to create a flat focal plane, matching the geometry of the prism expansion volume.

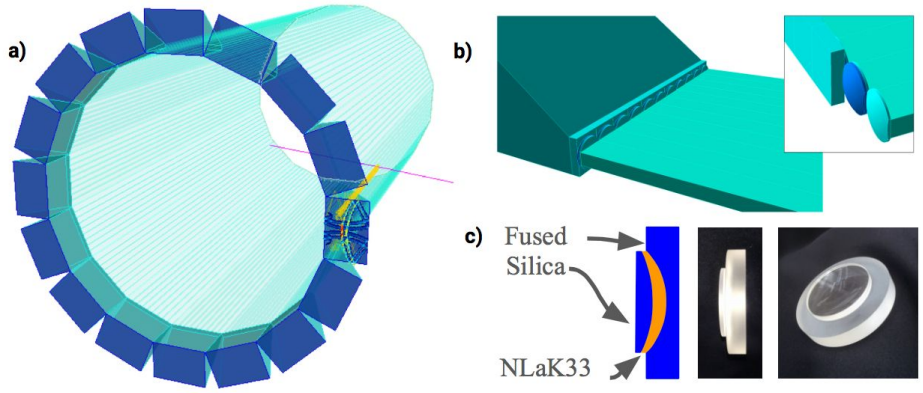

Figure 2.4.1: a) Geant4 geometry for the simulation of the high-performance DIRC. b) The fused silica prism expansion volume, a row of spherical three-layer lenses with high index of refraction (no air gaps) and the radiator bars. The insert shows the

individual lenses and layers of the spherical lens system. c) Schematic and photos of the 3-layer lens prototype.

2.4.1 Past

2.4.1.1 What was planned?

The key hardware-related activity planned for FY18 was to determine the performance of a new cylindrical 3-layer lens with particle beams and on test benches. Results of these studies are crucial to validate the wide plate geometry option for the High-Performance DIRC design.
We also planned to study the optical properties and radiation hardness of various DIRC materials used in the simulation by irradiating samples with X rays, Co^{60}, and neutrons at CUA. We also planned to resume simulation studies with the new postdoc, focusing on the time-based imaging reconstruction method for optimization of the bar/plate-based configurations - leading to a baseline design that can be fully implemented in the relevant EIC detector simulation frameworks. Additional goals were: Determination of the optimum pixel size of the sensors and the time resolution requirement for the high-performance DIRC using time-based imaging; Investigation of the chromatic dispersion mitigation in the context of different photocathode materials (for the narrow bar geometry); Study the potential use of the DIRC for high-precision event timing.

2.4.1.2 What was achieved?

Experimental validation of the performance of the new version of the 3-layer lens is crucial for the DIRC in the EIC R&D program. Pictures of the first prototype cylindrical lens that was procured in the end of FY17 are shown in Fig. 2.4.2. The design and fabrication were completed in the summer of 2017, just in time to place it in a particle beam at CERN as part of the scheduled PANDA Barrel DIRC prototype test. Since not all of the required components of the high-performance DIRC baseline design are available yet (such as sensors with small pixels, fast readout electronics, full-length radiators, *etc.*) the collaboration with the PANDA DIRC group was used to evaluate the performance of the 3-layer spherical lens as part of a prototype with their geometry.

The modular design of the PANDA Barrel DIRC prototype allowed for the easy exchange of several components between measurements to test their impact on the prototype performance. Several types of radiators, lenses, and imaging options were tested during the 2017 test beam campaign at CERN. Due to the larger pixel size of the MCP-PMTs available for the test beam (6.5-mm pixel pitch), the different length of the bar and size of the prism, the results from this test beam are not expected to agree with the performance predicted for the high-performance DIRC. However, the EIC DIRC simulation package can be used to translate the achieved performance to the EIC DIRC geometry.

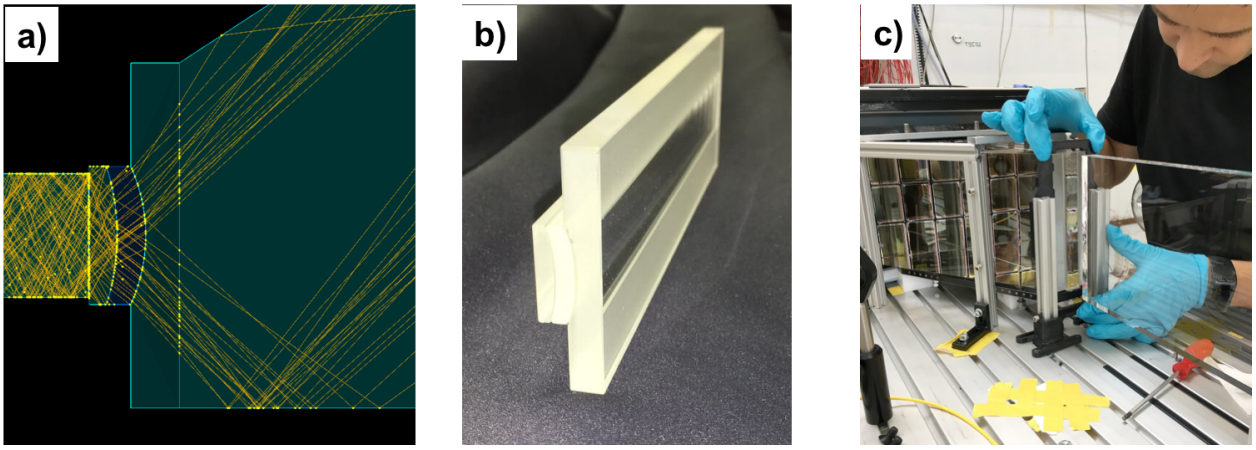

Figure 2.4.2: a) The new 3-layer cylindrical lens in Geant simulation; b) A photo of the lens in the lab; c) A photo of the lens installed in the PANDA Barrel DIRC 2017 prototype at CERN, placed between the wide radiator plate and the prism.

2017 test beam at CERN

The test beam at CERN in August/September 2017 was primarily focused on the validation of the PID performance of the geometry using wide radiator plates, with and without the 2-layer or 3-layer cylindrical lens. In addition, some time was dedicated to measurements with the narrow bar in combination with 3-layer spherical and cylindrical lenses. A picture of the setup used at CERN with the wide plate is shown in Fig. 2.4.2c. The radiator bar or plate was coupled to the 3-layer cylindrical lens or directly to the synthetic fused silica prism expansion volume with a 33° opening angle. The data analysis is still in the early stages but a preliminary result for the geometry with the narrow bar and the 3-layer lens is shown in Fig. 2.4.3. One should note that this result is obtained with a preliminary calibration and that the performance parameters are expected to improve with a more advanced analysis.

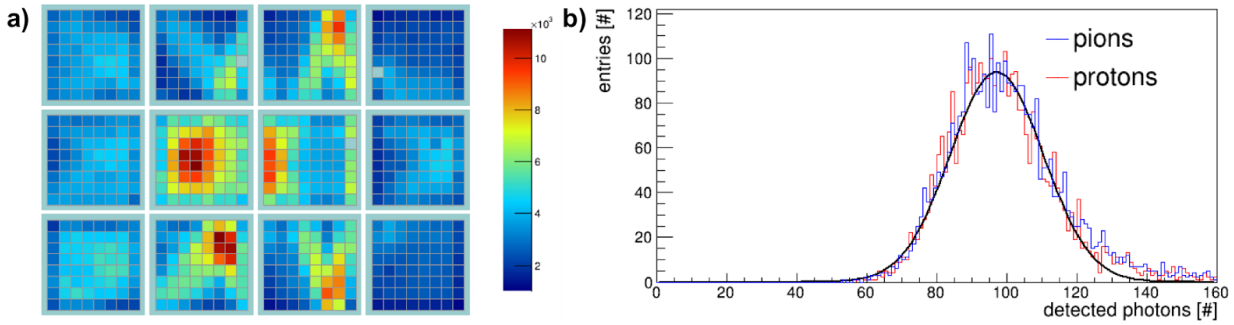

Figure 2.4.3: Preliminary result of the Prototype with 3-layer cylindrical lens from the 2017 CERN test beam: a) Distribution of the hits per MCP-PMT pixel from 50k events for tagged pions at a polar angle of 20° and a momentum of 7 GeV/*c*; b) photon yield for tagged pions and protons at a polar angle of 25° and a momentum of 7 GeV/*c*.

Radiation Hardness Measurement

The determination of the radiation hardness of materials is an important aspect of the EIC DIRC R&D. Synthetic fused silica, which is used for most of the optical components in all DIRC systems, was already extensively tested for the BaBar and PANDA DIRC counters and proved to be radiation hard. However, the middle layer of the 3-layer lens is made of a high-refractive index lanthanum crown glass, NLaK33, which had yet to be tested for radiation hardness.

The irradiation was performed at Catholic University of America in an X-ray setup with energies up to 160 keV. The dose was accumulated in small steps, delivering a dose of 50–100 rad at a time. To quantify the impact of the radiation, between each step, the transmission properties of the lens and a pure NLaK33 sample were measured in a monochromator setup with a reproducibility of 0.2%.

To disentangle the radiation damage effects of the composite materials (synthetic fused silica, NLaK33, epoxy glue, and anti-reflective coating), a pure NLaK33 sample was studied first. A synthetic fused silica sample served as a reference in the monochromator to remove systematic errors from the NLaK33 measurement. The 28x28x8 mm^3 sample of NLaK33 material was irradiated in the X-Ray setup set to 160 keV and 6.2 mA. Results of two measurement runs are shown in Fig. 2.4.4. The transmission drops significantly at a rate of around 1.3% per each 100 rad at 420 nm wavelength. During the first irradiation run the total deposited dose was 1 krad, resulting in 14% loss of transmission at 420 nm. Afterwards, the NLaK sample was left exposed to daylight at room temperature for 9 months. After this time, the transmission was measured again and a recovery of about 12%, to just 2% below the initial transmission, was observed. Further irradiation by an additional 5 krad showed that the transmission deteriorated at a similar rate as during the first run. The investigation of the annealing process has started and will continue as the recovery of the transmission may mean that NLaK33 remains a candidate for use in the EIC DIRC. As a next step we plan to irradiate NLaK33 samples with a Co60 source and with neutrons.

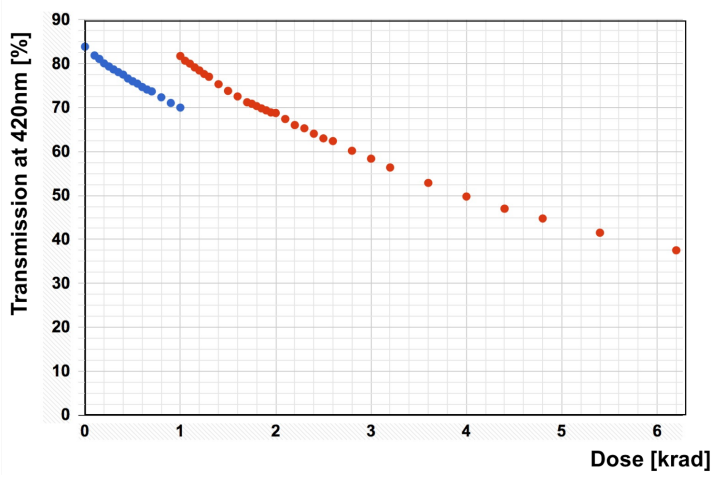

Figure 2.4.4: Measured transmission at 420 nm (not corrected for Fresnel losses) through the 8-mm thick NLaK33 sample as a function of X-ray irradiation dose. Blue points represent the first irradiation run with a dose up to 1 krad. The red points show the second run, adding an additional 5 krad dose nine months later.

2.4.1.3 What was not achieved?

The radiation hardness measurement of the 3-layer lens at CUA is in progress. The unexpected recovery of the NLaK33 glass sample is a very interesting effect that has to be studied carefully.

The new cylindrical 3-layer lens was sent to GSI immediately after fabrication to be included in the PANDA beam test at CERN, which delayed measurements of the lens properties on the test bench at CUA to the second half of FY18.

The hardware-related activities were given the highest priority in the first part of FY18 to make optimum use of the synergy with the PANDA DIRC beam test at CERN. This meant delaying the planned work on the improvement of the time-based imaging reconstruction method and on the simulation studies of the baseline design and the pixel size.

2.4.2 Future

2.4.2.1 What is planned for the rest of FY18? How, if at all, is this planning different from the original plan?

GSI is currently building a multi-axis rotation holder for the mapping of the focal plane of the new cylindrical 3-layer lens, which will be sent to CUA with the lens in January. The measurements of the lens properties at CUA will focus on the 3D focal plane measurements.

The NLaK33 samples will be studied further in terms of radiation hardness. That includes both the recovery after X-ray irradiation and irradiation with a Co60 source. We also plan to obtain samples of new potential alternative materials to NLaK33 and test those in our setups.

The activities on the detailed GEANT simulation and the time-based imaging are being picked up again after hiring the new PostDoc at CUA. The work will be shared with GSI and important next steps include the simulation of the new 3-layer cylindrical lens, improvements to the time-based imaging method, and the optimization of the lens design. A key near-term goal is the implementation of the High-Performance DIRC baseline design into the ePHENIX detector simulation framework.

2.4.2.2 What are the critical issues?

The radiation-hard 3-layer lens is a core element of the High-Performance DIRC design. The significant radiation damage of the NLaK33 material at a modest X-ray dose and the subsequent transmission recovery need to be studied in detail and alternate materials have to be identified. To facilitate the evaluation of the DIRC performance in combination with other PID systems, the optimization of the DIRC design and the implementation in existing detector simulation frameworks, like the ePHENIX framework, are crucial.

2.5 High Resolution Time-of-Flight

The high resolution TOF R&D (psTOF) aims to demonstrate that a 10-picosecond TOF system could be considered for particle identification at the EIC. Two detector technologies are investigated, multi-gap Resistive Plate Chambers (mRPC) and Micro-Channel Plate PMTs (MCP-PMT). In detector scenarios that have been envisioned for the EIC, 10-ps TOF would enable 3 sigma π/K and K/p separation at 3.5 and 6 GeV/*c*, respectively, in the barrel. In the forward (hadron) direction, at a distance of 3 m, one could achieve 6.5 and 11 GeV/*c* separation, respectively. TOF, in conjunction with a TPC, would aid in electron identification. It would also provide a start counter for DIRC detectors which require timing (aka, TOP detectors). High Resolution TOF may provide a more cost-effective and compact solution compared to other technologies.

2.5.1 Past

2.5.1.1 What was planned for this period?

The psTOF effort was funded with $5k to enable CCNY, with their electrical engineering expertise, to join our group by building a second prototype of our high-bandwidth fast preamp (the UFAMP). The original board was limited to 300 MHz analog bandwidth due to parasitic capacitances from test traces that were designed into the board. The strong effect from the parasitic capacitance was not originally expected. Also, we planned to pursue modifying the input circuit to provide better matching between the mRPC detector and the amplifier to reduce the reflection and oscillatory behavior that has been seen in the output signals.

2.5.1.2 What was achieved?

CCNY has involved quite a few undergraduate students and used the mating of the UFAMP with mRPC detectors as an instructional example of how to properly amplify small detector signals. Measurements of the detector capacitance and impedance were done, and used in the modeling of the input circuit to the UFAMP. In addition, the UFAMP circuit was modeled in LTSpice and optimized in order to produce the targeted 1-GHz bandwidth and voltage gain of about 16 (see Figures 2.5.1 and 2.5.2).

2.5.1.3 What was not achieved, why not, and what will be done to correct it?

We did not actually produce any new boards as of yet. The statement of work was completed in Nov/Dec, and we expect that we should be able to start producing prototypes of the revised UFAMP in early 2018.

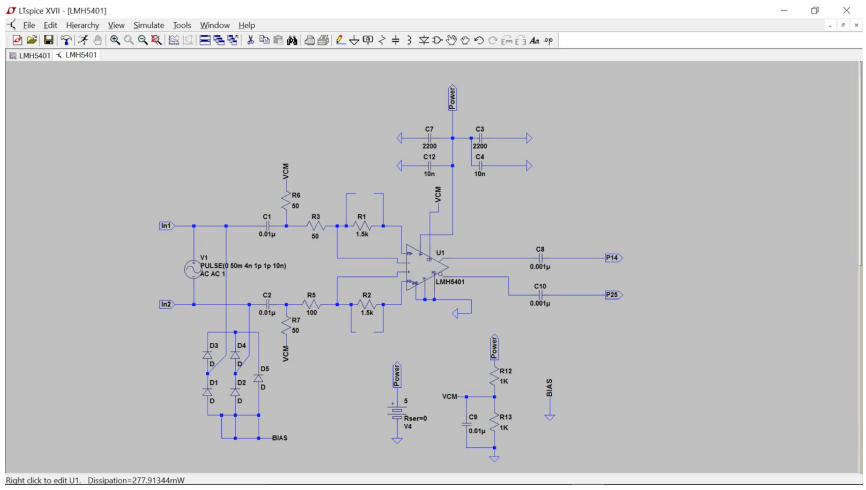

Figure 2.5.1: Improved UFAMP schematic from CCNY.

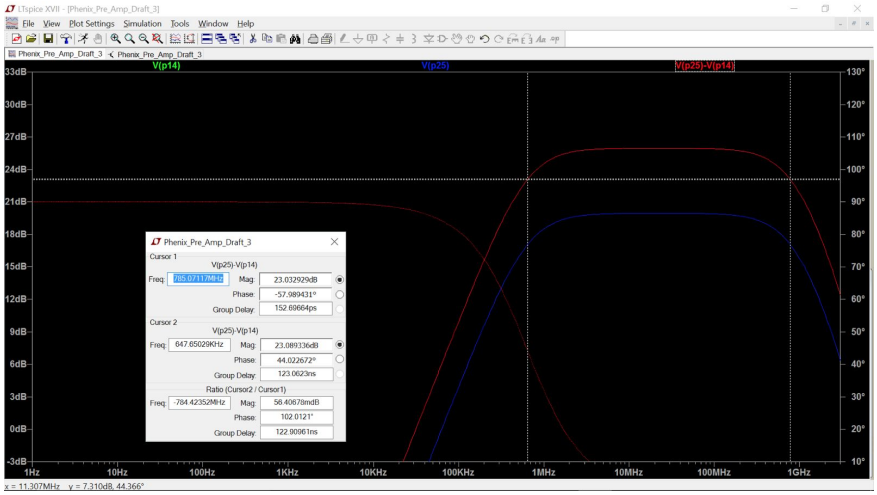

Figure 2.5.2: Response to an input step pulse of the improved UFAMP. Bandwidth reaches up to 1 GHz.

2.5.2 Future

2.5.2.1 What is planned for the next funding cycle and beyond? How, if at all, is this planning different from the original plan?

We are currently seeking external funding to produce the analog digitizer board based on the DRS4 ASIC through SBIR Phase I. This was originally proposed through the EIC R&D program but not funded, and therefore we are seeking external funds. The funding will go toward our goal of producing a small prototype, of 1-2 m^2, that will be tested in heavy ion collisions from RHIC at the sPHENIX detector starting in early 2023. The aim of this prototype is to demonstrate under realistic conditions TOF resolutions of 20 ps. We have already previously demonstrated that this is possible on a small scale in the lab, but the TOF resolution when scaling up to 1000's of channels and over several square meters needs to be also demonstrated.

PID capabilities would dramatically expand the physics scope of sPHENIX. Due to the very high multiplicities in heavy ion collisions, high-resolution TOF is the only detector technology capable of working in these collisions. There is significant interest from several groups across the world to fund development of high resolution TOF, so that if our R&D completes early enough we may be able to procure the funding for a full barrel 20-ps TOF in sPHENIX.

2.5.2.2 What are the critical issues?

We believe that the main impediment is of course funding support, which is why our planning now is leaning much more heavily toward securing separate funding from this program.

3. Photosensors and Electronics

3.1 Summary

The main objective of this R&D effort during the period July – December 2017 was to continue to identify and assess suitable photosensor solutions for the EIC Cherenkov Detectors and to develop electronics solutions for the readout of the Cherenkov detectors prototypes for beam tests. Ultimately, in the long term, this R&D work will allow us to make a recommendation about the best photosensors and electronics solutions for the PID detectors in EIC implementation.

3.2 Sensors in High-B Fields

3.2.1 Past

3.2.1.1 What was planned for this period?

In this reporting period we planned to measure the gain of Photonis Planacon(10-μm pore size) multi-anode MCP PMT as a function of B, θ, and φ. For definitions of θ, and φ, see Fig. 3.2.2. We also planned to begin development of an MCP-PMT simulation in order to study design optimizations to improve the MCP PMT performance in high B-fields; and to acquire equipment for timing-resolution measurements in high B-fields.

3.2.1.2 What was achieved?

In Summer 2017 the gain of Planacon (10-μm pore size) multi-anode MCP PMT was measured as a function of B and $\theta = 0^{\circ}$, 10°, and 20°. The results are shown in Fig.3.2.1. The data were obtained by illuminating only two detector channels. The gain increases at small field magnitudes and reaches a maximum at 0.3 T for all test orientations. Above 0.3 T the gain decreases as the B-field increases, however the rate of decrease increases as θ increases. The high voltage on the PMT at which the tests were done was 96% of the maximum recommended value.

The gain of the 10-μm Planacon was also measured as a function of B and θ for φ = 0°, 90°, 180°, and 270°. The results are shown in Fig. 3.2.2. All gains are normalized to the gain at B = 0 T, φ = 0°.

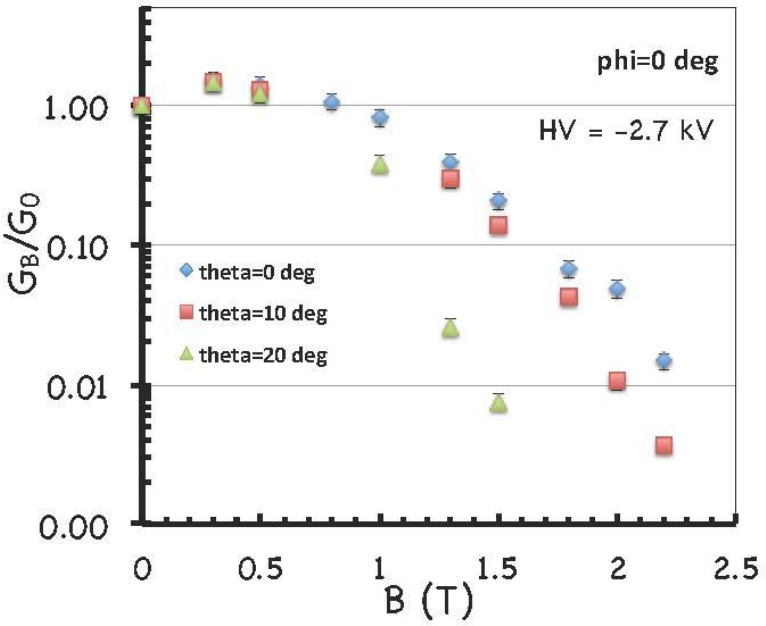

Figure 3.2.1: Relative gain of ch. 35 of 10-μm pore-size Planacon MCP PMT as a function of magnetic-field magnitude. θ is the angle between the normal to the PMT's front and the B-field vector. Above fields of 1.3 T the gain at θ=10° decreases faster with B than at 0°. Above fields of 1 T, the gain at θ=20° decreases faster with B than at 0° and at 10°. This narrows the maximum field at which the sensor can be operated at these orientations. The error bars show preliminary 14% uncertainties dominated by systematics.

The gain variation over φ is much weaker than the variations over θ and B. There are some interesting features, however. At θ = 0° the gain shows a slight dip at φ = 180° for all values of the B-field. A much more pronounced dip is observed at θ = 10°, but now at φ = 270° and, again, for all values of the B-field. The gain curves at θ = 20° do not show any characteristic trend as a function of φ.

Since the pulse-height spectra of this Planacon PMT have the single-photoelectron peak well separated from the pedestal up to B-field of 1 T, we could not only estimate the PMT gain from fits to these spectra, but also obtain the average number of photoelectrons, μ, for each setting (B, θ, φ = 0°). These results are shown on Fig. 3.2.3. The data show interesting features. While at θ = 0°, both the gain and the number of photoelectrons increase as the field increases to 0.3 -- 0.5 T and decrease at larger B, at the larger θ angles, the number of photoelectrons decreases steadily as the field increases and does not show a maximum at ~0.3 T as the gain. These trends suggest that at these larger θ angles not all photoelectrons emitted from the photocathode create an avalanche in the microchannel-plates. One hypothesis that could explain this effect is that the transverse B-field at these angles is sufficiently large so that the radius of curvature of the trajectory of some photoelectrons is too small for the photoelectrons to reach the first MCP. The data show that the larger θ is, the larger the loss is: about 25% at 10° and about 50% at 20°, which is qualitative consistent with the hypothesis. Simple calculations can be done, once the distance between the photocathode and the first PMT is known, to check if this explanation is reasonable. Above 0.3 T the loss of photoelectrons does not depend strongly on the B-field magnitude. To decrease the loss, one can increase the speed of the

photoelectrons by increasing the voltage between the photocathode and the first MCP. This can be experimentally tested in Summer 2018.

Our 2017 gain evaluation results show that the B-field, combined with the sensor orientation, affects not only the gain, but also the efficiency of the MCP-PMT and that both quantities need to be monitored in the assessment of MCP-PMT performance in high magnetic fields. The accurate extraction of both parameters, depends strongly on the quality of the MCP PMT, as it relies on fits to pulse-height distributions in which the single-photoelectron peak is well separated from the pedestal. In FY18, we will study alternative methods for simultaneous determination of *G* and *μ*, which could be applied to our previous measurements of other MCP PMTs where the fits could not be done over a broad range of *B* and *θ*.

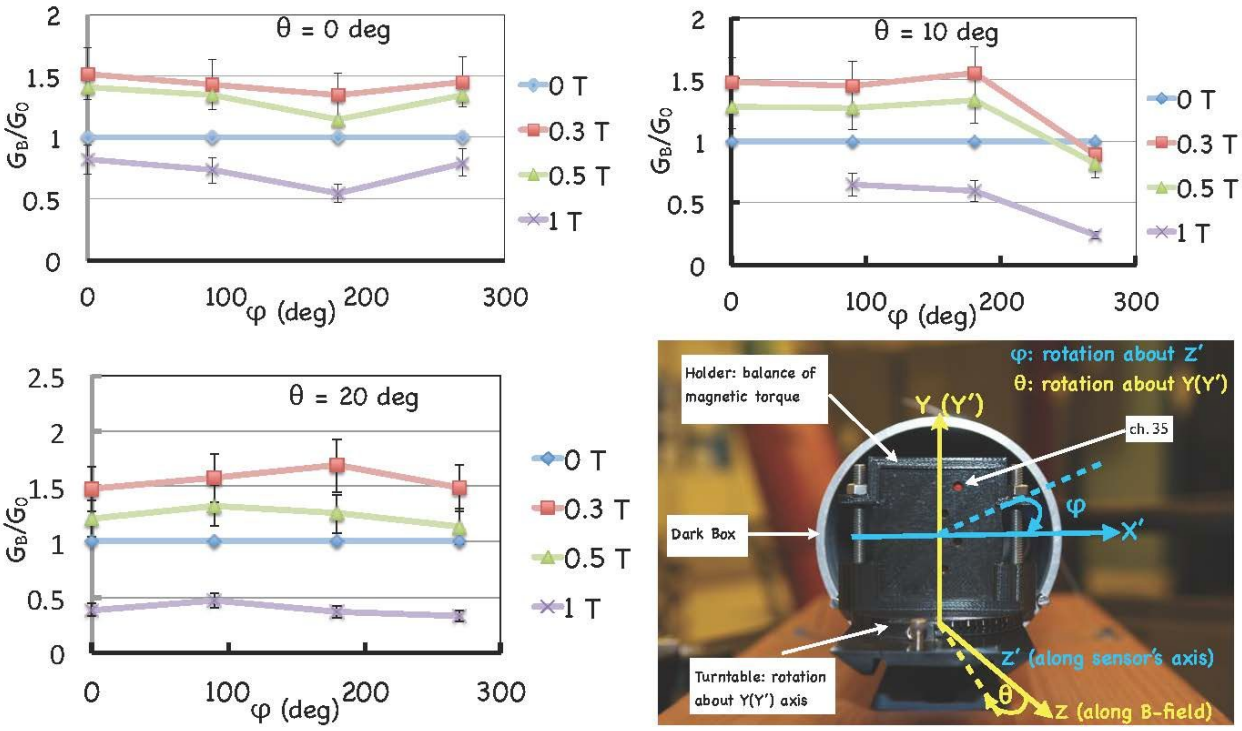

Figure 3.2.2: Relative gain of Planacon (10-μm pore size) MCP PMT as a function of *φ* for various *B* and *θ* (top left, top right, and bottom left). Bottom right: A picture of the MCP PMT in the dark box, showing the definitions of the rotation angles *θ* and *φ*. The error bars show preliminary 14% uncertainties dominated by systematics.

With respect to the upgrade of the JLab test setup to allow for timing measurements, we have purchased a fast laser (C. Hyde at ODU, non R&D funds) and optical components, such as digital attenuator, beam splitter, optical fibers, etc. (JLab, R&D funds). We will design and build an optical box for the laser and commission the system in 2018.

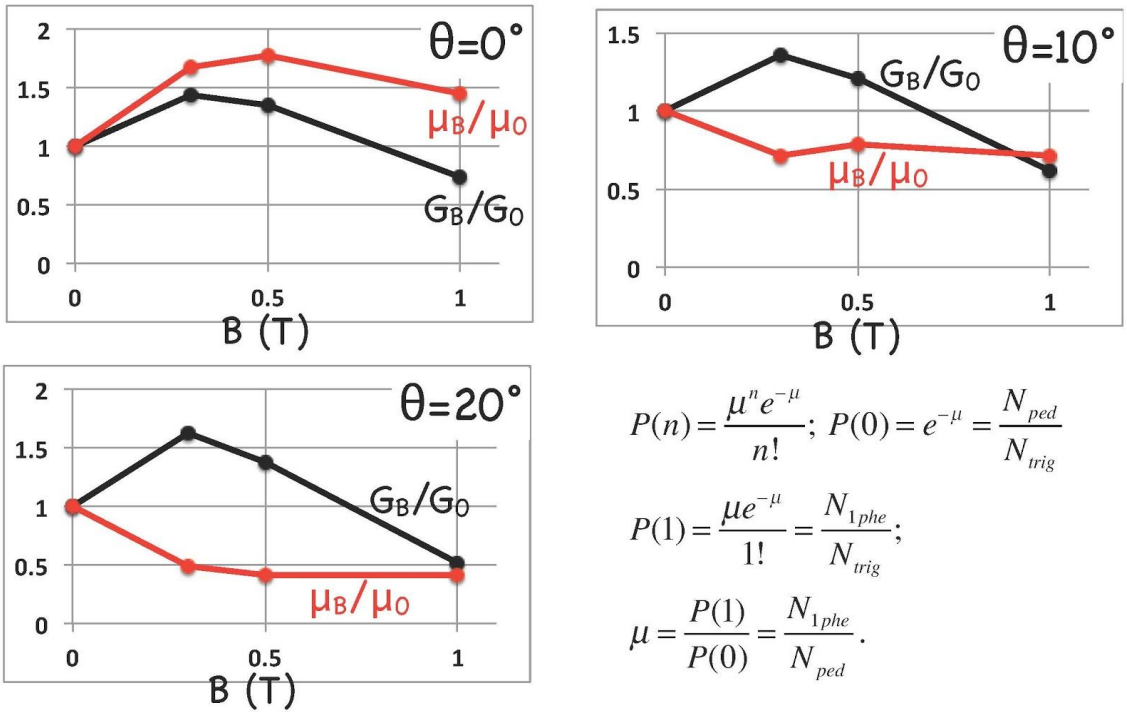

$$P(n)=\frac{\mu^n e^{-\mu}}{n!};\ P(0)=e^{-\mu}=\frac{N_{ped}}{N_{trig}}$$

$$P(1)=\frac{\mu e^{-\mu}}{1!}=\frac{N_{1phe}}{N_{trig}};$$

$$\mu=\frac{P(1)}{P(0)}=\frac{N_{1phe}}{N_{ped}}.$$

Figure 3.2.3: Red: Average number of photoelectrons (normalized to the number of pedestal events), μ, as a function of *B*-field and angle θ. **Black:** Gain, *G*, as a function of *B*-field and angle θ. Both *G* and μ are reported in units of the corresponding values at 0 T. In the equations in the bottom right, *P*(*n*) denotes the probability to observe *n* photoelectrons.

3.2.2 Future

3.2.2.1 What is planned for the next funding cycle and beyond? How, if at all, is this planning different from the original plan?

For the rest of FY 2018 we plan to (a) assess the extent to which the loss of gain of Planacon (10-μm pore size) multi-anode MCP PMTs for various (*B*, θ, φ) can be compensated by adjusting the individual HV across the three MCP-PMT stages: photocathode-MCP, MCP-MCP, and MCP-anode, especially, the first stage is of significant interest; (b) implement a timing upgrade to the test facility and perform first time-resolution measurements, and (c) continue to develop the MCP-PMT simulation. This plan does not differ from the original plan in terms of content. Due to restricted budget, some of the activities may not be completed in 2018.

3.2.2.2 What are the critical issues?

The availability of R&D funding at the beginning of the calendar year is critical in order to keep this program within the planned timelines.

3.3 LAPPDs

The LAPPD™ project is a multi-year project involving a number of institutions, with a goal to create an MCP-PMT that has the same very high performance as existing MCP-PMTs, but at a significantly lower cost. Specifically, for the EIC detector R&D, the effort aims to adapt the LAPPDs to the EIC requirements, which include pixelated readout and acceptable performance in high magnetic fields. With these adaptations, the LAPPDs can be used for the readout of mRICH, dRICH, and DIRC detectors, and for TOF applications.

3.3.1 Past

3.3.1.1 What was planned for this period?

For the period 7/1/17 – 12/31/17, we planned to complete the experimental performance testing and data analysis of small format (6cm x 6cm active area) micro-channel plate (MCP) photodetectors with standard LAPPD design in the Argonne G-2 magnet facility.

3.3.1.2 What was achieved?

In the summer of 2017, the ANL group tested the performance of 6cm x 6cm MCP-PMT at the Argonne G-2 magnet facility. The magnet provides a large bore with a diameter of 68 cm and a very homogeneous eld (7 ppb/cm), with a tunable strength of the magnetic field up to 4 T. A custom-built characterization system compatible with the solenoid magnet was built for this measurement, capable of characterizing large size MCP-PMTs up to 20 cm x 20 cm. A rotation mechanism was also integrated with the system, allowing rotation of the MCP photodetector at an angle θ, as shown in Fig. 3.3.2 (left). The MCP-PMT under testing is the 2nd version design with independent biased voltage for each MCP, so that the high voltage of each MCP can be optimized based on their resistance for best performance.

The dependence of the sensor performance on the magnetic field strength was done at a rotation angle $\theta = 0^o$, *i.e.*, where the direction of the magnetic field is normal to the surface of the MCP photodetector. We measured the performance of the investigated MCP photodetector in various magnetic field strengths at different bias high voltages. The results are presented in Fig. 3.3.1 (right). At a fixed bias high voltage, the mean pulse height of the MCP photodetector increases slightly as the magnetic field strength increases to 0.2 T, decreases as the magnetic field strength continues to increase as high as 0.8 T. In the same magnetic field environment, the mean pulse height of the MCP photodetector increases as the high voltage increases. This behavior is similar to our previous measurements of the MCP photodetectors without applying a magnetic field.

The magnetic field tolerance of the ANL version 2 independently-biased voltage MCP-PMT is compared with that of the ANL version 1 internal-resistor-chain design (Fig. 3.3.1 left), which was previously tested at JLab. The magnetic-field tolerance of the version 2 device is up to 0.8 T, which is greatly improved compared to that of the version 1 design of up to only 0.2 T. The

great improvement indicates that the optimization of the bias voltage for each MCP is very important for the device's magnetic-field tolerance. The current MCP-PMT magnetic-field tolerance performance is very encouraging and the result is comparable to that of current commercially available MCP-PMTs (~1.0 T) with similar pore size. Here, we must emphasize that the current LAPPD design is not yet optimized for magnetic-field tolerant applications. The distances between the photocathode, MCPs, and the anode are relatively large in the LAPPD design. For instance, the spacing between the photocathode and the top MCP is 2 mm and spacing between the bottom MCP and the anode is 3.2 mm. To optimize for a magnetic field environment, these distances should be reduced to minimize the electron transit distance. Meanwhile, MCP photodetectors with smaller pore sizes have shown better magnetic field tolerance than those with larger pore sizes. A redesign of the current LAPPD configuration with smaller pore sizes (*e.g.*, 10 μm or even 5 μm) and reduced distances between the PMT elements should significantly improve its magnetic field tolerance.

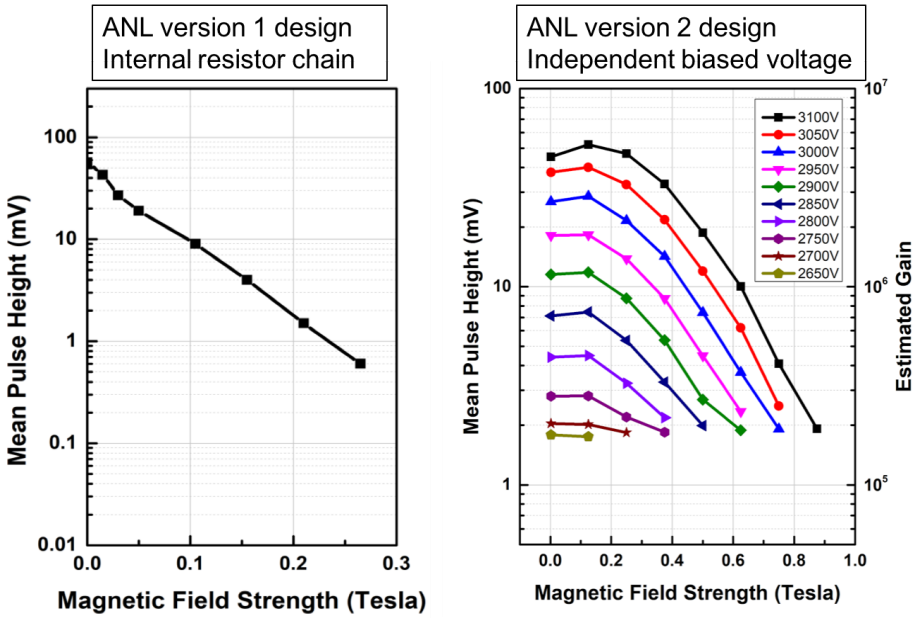

Figure 3.3.1: MCP-PMT mean pulse height dependence of magnetic field strength: (left) the ANL version 1 internal-resistor-chain design, (right) the ANL version 2 independent-biased voltage design. Obvious improvement is achieved by independently bias the high voltage of each MCP.

The angular dependence of the MCP photodetector magnetic-field tolerance was additionally studied by rotating the MCP photodetector at angle θ relative to the magnetic field direction, as shown in Fig. 3.3.2 (left). We fixed the bias high voltage at 3000 V on the photodetector and rotated the photodetector from −90° to +90° for a full range of angle measurements. Figure 3.3.2 (right) presents the response of the MCP photodetector, in terms of the mean pulse height, measured as a function of the rotation angle θ at two magnetic field strengths of 0.25 and 0.5 T. For $\theta < -30^\circ$ or $\theta > 30^\circ$, any signal is hardly separated from the noise level. Within $-30^\circ < \theta < 30^\circ$, there are two peaks at about $\theta = \pm 8^\circ$, which are due to the chevron configuration of the two

MCPs inside the photodetector. The detector's response reaches a maximum when the pore of either MCP is well-aligned with the magnetic field direction. The intensities of the two peaks are different, which is due to the different effect from the top and bottom MCPs.

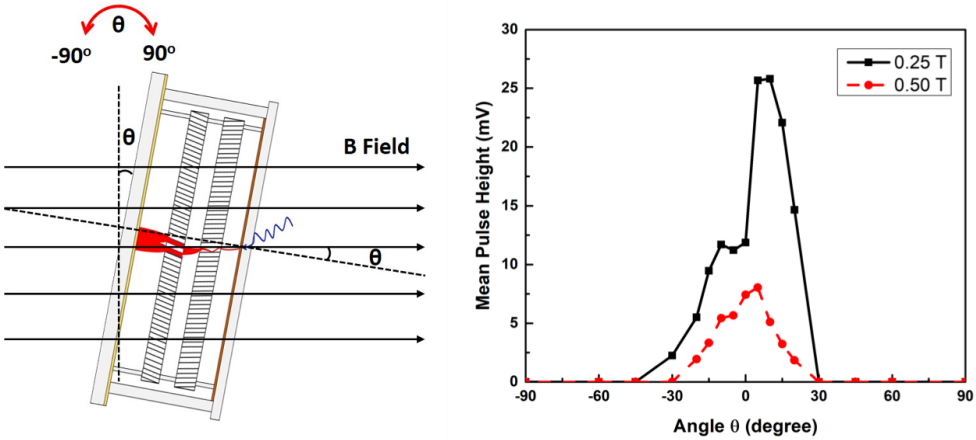

Figure 3.3.2: (left) Schematic of the rotation mechanism of the MCP photodetector. (right) Response of the MCP photodetector as a function of the rotation angle θ relative to the direction of magnetic field. The two peaks around -8^{o} and 8^{o} indicate the effect due to the 8^{o} bias angle of the MCPs. Note that the intensities of the two peaks are not the same due to the different effect from top and bottom MCPs.

3.3.2 Future

3.3.2.1 What is planned for the next funding cycle and beyond? How, if at all, is this planning different from the original plan?

In the rest of FY2018, we plan to continue MCP-PMT fabrication and characterization work as scheduled:

- Complete MCP-PMT stack in vacuum with capacitive coupling readout for beamline test
- Produce a modified MCP-PMT with smaller pore size and reduced spacing between components for testing.
- Test the magnetic field tolerance of the newly produced MCP-PMTs.

3.3.2.2 What are the critical issues?

Shortness of funding support is continuously the major issue for the ANL MCP-PMT project. The project was previously funded through DOE-HEP detector R&D funding. Since FY17, the Office of HEP at DOE has determined to wind down its support of the LAPPD project since Incom. Inc has started the pilot production and commercialization of LAPPDs. This reduced the funding support for the ANL-LAPPD project by ~1M. The optimization of LAPPD MCP-PMTs is now supported by fractional funding from Argonne LDRD and EIC detector R&D funding to keep the program ongoing at a minimum spending. An SBIR phase I proposal was submitted this year in collaboration with Incom Inc. aiming to optimize the LAPPD design for high-magnetic field

tolerance LAPPD for EIC PID application.

3.4 Readout Sensors and Electronics for Detector Prototypes

3.4.1 Past

The data acquisition system for the first mRICH beam test was provided by the INFN group led by Marco Contalbrigo. There were four Hamamatsu H12700A modules mounted at the sensor plane. The H12700A readout consisted of three circuit boards as described in http://infn.fe.infn.it/~mcontalb/JLAB12/RICH_midterm_review/RICH_Electronics_Turisini.pdf. The adapter board is a passive board mounting connectors to couple the MA-PMTs socket to the electronics. The ASIC board is based on the MAROC3 chip by OMEGA described in http://omega.in2p3.fr/index.php/download-center/doc_details/393-proceedingsieeenss2010maroc3.html served by voltage regulators (Analog Devices AD5620). The FPGA board is based on the Xilinx Artix7 and uses the Finisar FTE8510N1LCN optical transceiver to connect to a N-GXE-LC-01 fiber gigabit Ethernet to PCI express bus adapter in the readout computer.

The electronics for DIRC beam tests at CERN were mostly provided by the PANDA DIRC group as part of the GSI infrastructure that was made available to the EIC R&D program (although some compatible items were also procured as part of eRD4 prior to formation of the eRD14 consortium).

3.4.1.1 What was planned for this period?

The development of the readout electronics follows a multi-stage strategy. The goal is to provide a solution for all PID detector R&D needs, and a template for a final system to be used in the full EIC detector. The detailed schedule is adapted to the planned R&D schedule of each system. To experimentally demonstrate the PID performance, the DIRC prototype will eventually have to be instrumented with small-pixel sensors with good timing (<100 ps), which will require the next-generation SiREAD chip from U. Hawaii / Nalu Scientific, which is currently developed with SBIR funding. This would ideally happen after the prototype is moved to the U.S. However, the current round of component (lens) studies can be carried out using the sensors and electronics available at GSI. The initial priority is thus to develop a readout for the RICH detectors, and in particular the mRICH, for which a beam test is planned in the first half of 2018. The similarity between the sensors considered for the dRICH and mRICH also allows the latter to serve as a (sensor and readout) prototype for the former. It is our hope that even if the detailed requirements of the two systems would eventually diverge somewhat, a high degree of commonality can be retained. We also plan to use SiREAD for the next iteration of the readout for the RICH detectors – allowing for further synergies.

The primary goal for this reporting period was the development of a readout for the upcoming mRICH beam test, which will follow the very successful mRICH beam test at Fermilab in April 2016. The goal of the new beam test is to verify the PID capability by using new photosensors with finer pixel size (3mm x 3mm) from Hamamatsu: H13700A multi-anode PMTs and an MPPC

(SiPM) array. For this test, there is no requirement for <100 ps timing (which the CLAS12 electronics cannot fulfill). The availability of two prototypes and the need to test two types of sensors naturally led to a solution where one prototype would use a readout based on an evolution of the tested CLAS12 electronics provided by the INFN group ((M. Contalbrigo) and one based on the sampling electronics from the U. Hawaii group (G. Varner) and Nalu Scientific, LLC (I. Mostafanezhad). The latter is based on the TARGETX chip used in the electronics provided by that group for the Belle II upgrade at KEK. While the goal is to eventually switch over to the new SiREAD chip, the experience gained with an intermediate version based on TARGETX, as well as the cross reference with the CLAS12 electronics, will be an important part of the R&D process. The 64-channel SiREAD chip is currently being developed by Nalu Scientific, a small business specializing in System-on-Chip data acquisition systems, which has recently been awarded multiple DOE Phase I and Phase II SBIRs to develop the next generation readout electronics for HEP/NP applications. The goal is to have the readout electronics (both INFN/CLAS12 and Hawaii/TARGETX) ready for test in late spring 2018.

3.4.1.2 What was achieved?

U. Hawaii (G. Varner) has partnered with Nalu Scientific to develop a readout solution for mRICH using new readout ASICs. While the SiREAD chip is in the fabrication queue, a rev 1.0 PCB level design has been developed using the existing TARGETX chip. Such a design allows to rapidly test the electronic performance of readout scheme when coupled with the PMT or SiPM array. Figure 3.4.1 shows a rendering of the design to read out a 256-channel H13700 PMT and an expanded version to read out 1024 channels for the 2018 beam test. The PCBs have been designed and are awaiting a final design review to be sent to the fabrication house for manufacture. The project is on schedule for a 2018 beam test at Fermilab. If there is a decision to move to a SiPM array, the design is inherently flexible enough to allow such migration with minimal amount of redesign.

In parallel, the INFN group worked on upgrading the readout electronics (based on the JLab CLAS12 RICH electronics) for reading out the high channel density H13700 modules and explored the option for using SiPM array with cooling. The progress is on track. This may allow us to test both photosensors during the next mRICH beam test.

3.4.2 Future

3.4.2.1 What is planned for the next funding cycle and beyond? How, if at all, is this planning different from the original plan?

The consortium is developing readout electronics for future R&D needs. The plan is on track and will result in a system that can satisfy the needs of all the Cherenkov detectors (DIRC, dRICH, mRICH). The first version will be supplied for the mRICH beam test at Fermilab in the first half of 2018.

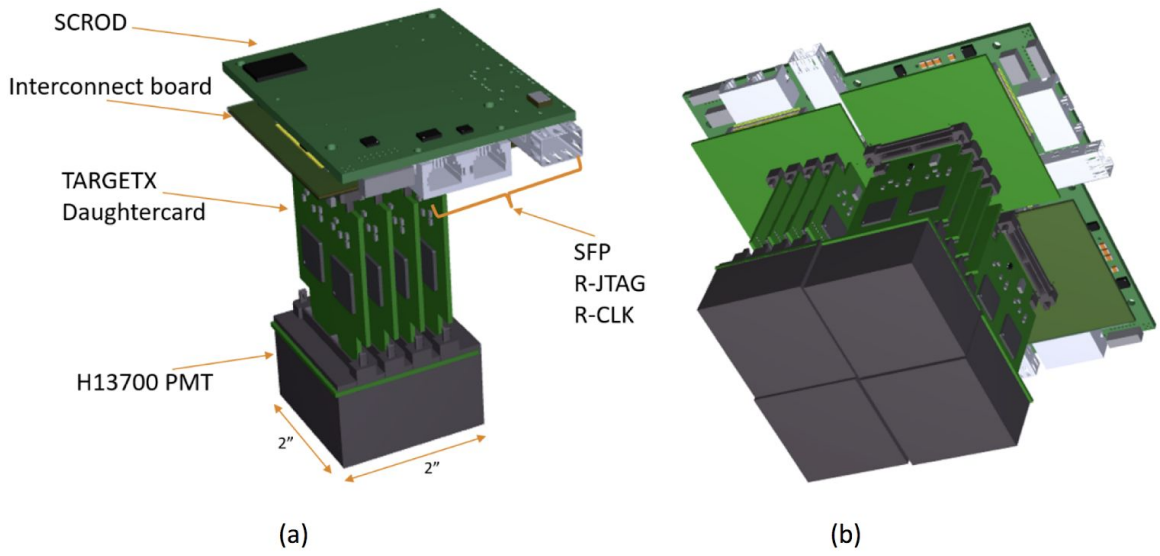

Figure 4.3.1: 3D rendering of the readout electronics proposed for H13700 PMT. (a) single PMT readout for 256 channels, and (b) four modules abutted to read out 1024 channels.

4. Manpower

Abilene Christian University

Rusty Towell, Faculty, 25% of time spent on project

Matt Kimball, Haley Stien, Aric Tate, Cecily Towell, undergraduate, 0.25 FTE, summer research at BNL, supervised by R. Towell and M. Chiu

Argonne National Laboratory

Bob Wagner, Staff Scientist, 10% of time spent on project, No FTE

Lei Xia, Staff Scientist, 15% of time spent on project, No FTE

Junqi Xie, Staff Scientist, 25% of time spent on project, 0.14 FTE

Mohammad Hattawy, Postdoctoral Appointee, 25% of time spent on project, No FTE

Tim Cundiff, Engineer, 10% of time spent on project, 0.07 FTE

Brookhaven National Laboratory

Mickey Chiu, Staff Scientist, 40% of time spent on project

Andrey Sukhanov, Electronics Engineer, 0.10 FTE

Rob Pisani, Scientific Associate, 0.25 FTE

Catholic University of America

Grzegorz Kalicy, Faculty, 50% of research time on project

Marie Boer, Postdoc, 50% of research time on project, supervised by G. Kalicy

Duke University

Zhiwen Zhao, Research professor

Georgia State University

Xiaochun He, Faculty, 30% of time spent on project.

Murad Sarsour, Faculty, 10% of time spent on project.

Cheuk-Ping Wong, Ph.D. student, 20% of time on the project, supervised by X. He.

Xu Sun, new postdoc, 40% of time on the project, supervised by X. He.

William Roh, new graduate student, 60% of time on the project, supervised by X. He.

GSI Helmholtzzentrum für Schwerionenforschung GmbH

Roman Dzhygadlo, Postdoctoral Research Associate, 25% of time spent on project

Carsten Schwarz, Staff Scientist, 15% of time spent on project

Jochen Schwiening, Senior Staff Scientist, 15% of time spent on project

Howard University

Marcus Alfred, Faculty, 25% of time spent on project

John Blakley, Kahlil Dixon, Robert Neblett, undergraduate, 0.25 FTE, summer research at BNL, supervised by M. Alfred and M. Chiu

Jefferson Lab

Carl Zorn, Staff Scientist

Los Alamos

Hubert van Hecke, Staff Scientist

Old Dominion University

Charles Hyde, Faculty, 30% of research time on project

Lee Allison, Doctoral Student, 100% on project (graduated in 2017), located at ODU/JLab and supervised by C. Hyde and G. Kalicy

Stony Brook University

Pawel Nadel-Turonski, Adjunct Professor, 30% of research time spent on project

University of Illinois at Urbana-Champaign

Matthias Grosse-Perdekamp, Faculty, 10% of time spent on project

University of South Carolina

Yordanka Ilieva, Faculty, 30% of time spent on project

Alessio DelDotto, Postdoctoral Fellow, 100% of time spent on project

Joshua Rapoport, Undergraduate Student, 17% of time spent on project (8 weeks), located at Jefferson Lab, supervised by Y. Ilieva, C. Zorn, and J. McKisson

Colin Gleason, Graduate Student, 5% of time spent on project (2 weeks), located at Jefferson Lab, supervised by Y. Ilieva

Include a list of the existing manpower and what approximate fraction each has spent on the project. If students and/or postdocs were funded through the R&D, please state where they were located and who supervised their work.

5. External Funding

ANL

- ANL-LDRD project: A Strategic Scientific Program to establish Argonne Leadership in the Development of the Future Electron-Ion Collider, Oct 1, 2017 – Sep 30, 2018: 10K

ODU

- University funds for fast (picosecond) laser pulser procurement for High-B timing measurements: $15k.
- University funds for travel for CERN PS test beam, Oct 10 - Nov 3, 2016: $4k.
- DOE Grant funding for Graduate Research Assistant, 100% on project: $19,000 (including indirect costs), 1 July 2016 — 31 December 2017

GSU

- University funds provided the major portion of the support for a graduate student and the research staff. We also used the university funds for purchasing building materials of constructing the mRICH prototypes and the supporting frames.

GSI

- Mechanical and DAQ components for the 2017 DIRC prototype: $10k.
- Travel for DIRC prototype beam test at CERN PS, Aug 23 - Sep 13, 2017: $20k.

INFN-Ferrara

- Development of higher density readout electronics moving towards the compatibility with 3 mm sensors (such as the ones required for the mRICH prototype): $6.5k.

See also the respective sections for more details on TOF, photosensors, etc.

6. Publications

6.1 In Preparation

X. He, *Ring Imaging Cherenkov Detector Technologies for Particle Identification in the Electron-Ion Collider Experiments,* The Proceedings of the 21st Particles and Nuclei International Conference, to be published in International Journal of Modern Physics: Conference Series.

Y. Ilieva, *Particle Identification for a Future EIC Detector,* Proceedings of DIRC2017: Workshop on Fast Cherenkov Detectors, to be published in Journal of Instrumentation.

G. Kalicy, *The High-Performance DIRC for a Future EIC Detector*, Proceedings of DIRC2017: Workshop on Fast Cherenkov Detectors, to be published in Journal of Instrumentation.

6.2 Recently Published or Submitted

A. Del Dotto et al., *Design and R&D of RICH detectors for EIC experiments*, poster at RICH2016 (9th International Workshop on Ring Imaging Cherenkov Detectors), September 5–9, 2016, Bled, Slovenia, published in Nucl. Instrum. Meth. A 876, 237 (2017).

C.P. Wong, et. al., *Modular focusing ring imaging Cherenkov detector for electron-ion collider experiment*, Nucl. Instrum. Meth. A 871, 13 (2017).

J. Xie et al., *Rate capability and magnetic field tolerance measurements of fast timing microchannel plate photodetectors*, Nucl. Instrum. Meth. A (in press). https://doi.org/10.1016/j.nima.2017.10.059

7. Presentations

C.P. Wong, *A Novel Modular Ring Imaging Cherenkov (mRICH) Detector for the Experiments in the Electron-Ion Collider*, IEEE Nuclear Science Symposium, 21–28 October, Atlanta, GA, 2017.

X. He, *Ring Imaging Cherenkov Detector Technologies for Particle Identification in the Electron-Ion Collider Experiments,* The 21th Particles and Nuclei International Conference, September 1–5, IHEP, Beijing, China, 2017.

Y. Ilieva, *Particle Identification for a Future EIC Detector,* DIRC2017: Workshop on Fast Cherenkov Detectors, 7–9 August, Castle Rauischholzhausen, Germany, 2017.

G. Kalicy, *The High-Performance DIRC for a Future EIC Detector*, DIRC2017: Workshop on Fast Cherenkov Detectors, 7–9 August, Castle Rauischholzhausen, Germany, 2017.